The Journal of Experimental Biology 212, 4002-4009
Published by The Company of Biologists 2009
doi:10.1242/jeb.034801

Elastic energy storage in the mantis shrimp's fast predatory strike

T. I. Zack*, T. Claverie† and S. N. Patek†,‡

Department of Integrative Biology, University of California, Berkeley, CA 94720-3140, USA

*Present address: Biophysics Program, Harvard University, Cambridge, MA 02138, USA
†Present address: Biology Department, University of Massachusetts, Amherst, MA 01003, USA
‡Author for correspondence (patek@bio.umass.edu)

Accepted 8 September 2009

SUMMARY

Storage of elastic energy is key to increasing the power output of many biological systems. Mantis shrimp (Stomatopoda) must store considerable elastic energy prior to their rapid raptorial strikes; however, little is known about the dynamics and location of elastic energy storage structures in this system. We used computed tomography (CT) to visualize the mineralization patterns in *Gonodactylaceus falcatus* and high speed videography of *Odontodactylus scyllarus* to observe the dynamics of spring loading. Using a materials testing apparatus, we measured the force and work required to contract the elastic structures in *G. falcatus*. There was a positive linear correlation between contraction force and contraction distance; alternative model tests further supported the use of a linear model. Therefore, we modeled the system as a Hookean spring. The force required to fully compress the spring was positively correlated with body mass and appendage size, but the spring constant did not scale with body size, suggesting a possible role of muscle constraints in the scaling of this system. One hypothesized elastic storage structure, the saddle, only contributed approximately 11% of the total measured force, thus suggesting that primary site of elastic energy storage is in the mineralized ventral bars found in the merus segment of the raptorial appendages. Furthermore, the intact system exhibited 81% resilience and severing the saddle resulted in a non-significant reduction to 77% resilience. The remarkable shapes and mineralization patterns that characterize the mantis shrimp's raptorial appendage further reveal a highly integrated mechanical power amplification system based on exoskeletal elastic energy storage.

Key words: biomechanics, feeding, Crustacea, springs.

INTRODUCTION

Skeletal muscle limits the power and speed of animal movements (Pennycuick, 1968; Asmussen and Marechal, 1989; Josephson, 1993; James et al., 2007). However, some animals have evolved power amplification mechanisms to circumvent this inherent restriction (Alexander and Bennet-Clark, 1977; Alexander, 1983; Alexander, 1990; Gronenberg, 1996). Biological power amplification is defined as a mechanism that decreases the amount of time to perform work. For example, by preventing joint rotation during muscular contraction, skeletal structures can channel work into elastic materials; when these structures are allowed to relax to their resting state, energy is released over a much shorter time scale than the underlying muscle contraction, thereby resulting in power amplification (Rothschild et al., 1972; Heitler, 1974; Roberts and Marsh, 2003; James et al., 2007). The use of elastic structures to amplify the power output of skeletal muscle is fundamental to rapid accelerations in animals (James et al., 2007).

A wide range of structures have been co-opted for elastic energy storage (Bennet-Clark, 1976a; Bennet-Clark, 1976b). In vertebrates, elastic energy is typically stored in the connective tissues associated with the contracting muscle (Alexander, 1984; Alexander, 2002) as well as other peripheral structures, such as gecko setae (Gravish et al., 2008). In these systems, the muscles act in series with a biological spring, which translates work to the relevant joint in less time than would be possible with the muscle contracting alone. Arthropods typically use elastic energy storage structures built from exoskeleton, connective tissue and rubbery resilin materials (Jensen and Weis-Fogh, 1962; Rothschild et al., 1972; Patek et al., 2007). For example, locusts store elastic energy prior to a jump by bowing a leg segment and then allowing it to spring back to its relaxed position during the jump (Jensen and Weis-Fogh, 1962; Heitler, 1974).

Although the functional morphology of power-amplified systems has been described in numerous arthropods (Bennet-Clark and Lucey, 1967; Bennet-Clark, 1975; Brackenbury and Hunt, 1993; Josephson and Stokes, 1994; Burrows, 2007; Burrows and Sutton, 2008), far fewer studies have analyzed mechanical dynamics of loading and release of elastic structures (Katz and Gosline, 1992; Katz and Gosline, 1994; Dudek and Full, 2006; Sachs et al., 2006). Dudek and Full (Dudek and Full, 2006) described the cycling dynamics of the cuticle of cockroach legs, showing that it may function as an energy-conserving spring in high speed running. Raabe et al. characterized the dynamics of lobster (*Homarus americanus*) endocuticle using tensile tests and the effect of water on specimen durability (Raabe et al., 2005). Several studies have examined the arthropod-specific scaling issues in the elastic energy storage mechanism in locust legs (Katz and Gosline, 1992; Katz and Gosline, 1994). Few, if any, other arthropod springs have been isolated and directly tested for their dynamic behavior during loading and release of elastic energy.

Depending on their mechanical behavior, elastic structures can be modeled many different ways, from the simplest Hookean spring, to more complex time- and distance-dependent springs (Blickhan, 1989; Blickhan and Full, 1993; Roberts and Marsh, 2003). By matching a mathematical model to the spring behavior, it is possible to derive other properties of the system, such as the time dependent velocity, acceleration, and elastic potential energy stored, as well as model variation within and among species.

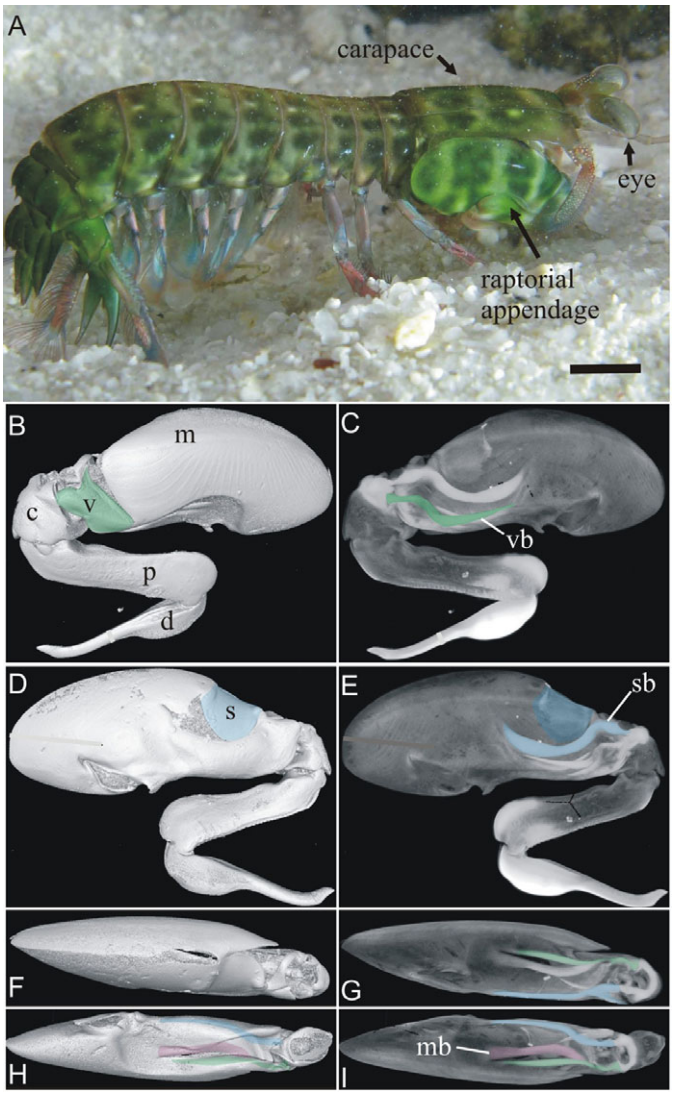

Fig. 1. *Gonodactylaceus falcatus* (A) uses its raptorial appendages to smash hard-shelled prey. Isosurface rendering (left column) and maximum projection (right column) were used to visualize surface conformation and mineralization from micro-CT scans, respectively. A lateral view of the left appendage (B) shows the component parts of the raptorial appendage: merus (m), meral-V (v), carpus (c), propodus (p) and dactyl (d). The exoskeletal shape of the meral-V (green, B) has little correspondence to the mineralized ventral bar (vb) that extends the length of the meral-V and proximoventrally along the merus (green, C). Similarly, isosurface rendering of the medial side of the raptorial appendage (D) shows the exoskeletal surface shape of the saddle (blue, s), but the mineralization in that region (sb, blue, E) actually extends ventrally to the saddle and connects distally to the carpus with very small regions of mineralization at the proximal and distal limits of the saddle. These same regions of mineralization are visible from a dorsal view (F,G, distal to right) and ventral view (H,I, distal to right). In the ventral view of the mineralization patterns (I), three mineralized regions are visible: the meral-V ventral bar (green), the saddle's medial bar (blue) and a centralized ventral region that runs along the midline of the appendage (mb, purple). Scale bar, 0.5 cm. The cross-hatch in E is an artifact of the imaging program.

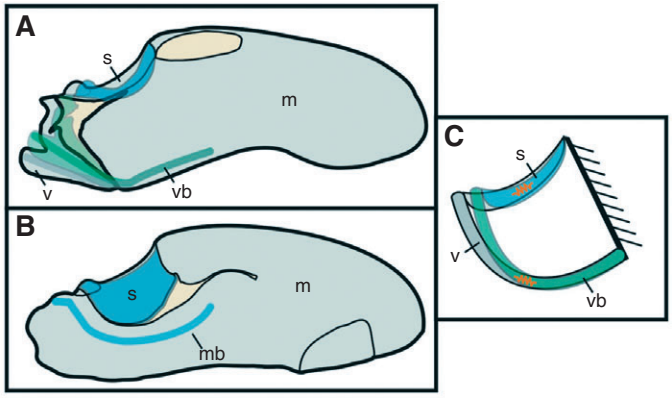

Fig. 2. During preparation for a strike, the merus moves from its resting position (solid outline) to a compressed state (overlaid colors) that was mimicked by our materials testing apparatus. (A) Visible on the outer lateral exoskeleton, the meral-V (green) rotates proximally and the saddle compresses and shortens in length (blue). Visible only through micro-CT scans, the mineralized ventral bar (green) must also flex as the meral-V rotates. (B) Also visible only through micro-CT scans, a mineralized medial bar extends along the ventral-medial edge of the saddle and connects at the meral–carpal joint. (C) The elastic energy storage mechanism tested here involves flexing the ventral bar and shortening the saddle during meral-V rotation. Proximal is to the right and dorsal toward the top of the page in all images. m, merus; s, saddle; v, meral-V; vb, ventral bar; mb, medial bar. Gray coloration indicates exoskeleton; tan coloration indicates arthrodial membrane. Images adapted from Patek et al. (Patek et al., 2007).

The location and dynamics of elastic energy storage have remained uncertain in the potent power-amplified system found in mantis shrimp (Crustacea: Stomatopoda; Figs 1, 2) (Burrows, 1969; Currey et al., 1982; Alexander, 1983; Patek et al., 2004). Mantis shrimp use their second thoracic appendages, called raptorial appendages, to produce extremely fast and forceful feeding strikes (Fig. 1) (Burrows, 1969; Patek et al., 2004; Patek and Caldwell, 2005; Patek et al., 2007). The key power amplification mechanism is a pair of sclerites (latches) that brace the meral–carpal joint during contraction of extensor muscles (Burrows, 1969; Patek et al., 2007). Once the sclerites are engaged, the strong and slow extensor muscles contract and compress the merus exoskeleton along its proximal–distal axis (McNeill et al., 1972; Patek et al., 2007). When the sclerites are released, the merus springs back to its original shape, forcing the carpus, propodus and dactyl to rotate with high acceleration (Burrows, 1969; McNeill et al., 1972; Patek et al., 2004; Patek et al., 2007).

Two key structures have been identified as probable energy storage structures – the meral-V and saddle (Fig. 2). Using computed tomography (CT), Patek et al. (Patek et al., 2007) identified a "ventral bar" of exoskeleton that extended from the meral-V (Fig. 2) to the ventral surface of the merus in the peacock mantis shrimp (*Odontodactylus scyllarus*). The meral-V rotates proximally during spring loading and rapidly rotates distally during the predatory strike (Patek et al., 2004; Patek et al., 2007). The rotation of the meral-V flexes the ventral bar, much like a tape spring (Seffen and Pellegrino, 1999; Vincent and Wegst, 2004), and acts as part of a four-bar linkage system to couple stored elastic energy to the rapid rotation of the carpus (Patek et al., 2004; Patek et al., 2007). Concurrent with the meral-V proximal and distal rotations during the preparation for and actuation of the strike, the saddle (an exoskeletal hyperbolic-paraboloid on the dorsal surface of the merus; Fig. 2) compresses and releases, respectively (Patek et al., 2004; Patek et al., 2007). However, CT scans indicated that the saddle is poorly mineralized and appears unlikely to store substantial elastic energy (Patek et al., 2007). The energy storage capacity had yet to be tested in any of these structures.

The primary goal of this study was to measure and characterize elastic energy storage in the mantis shrimp's raptorial appendages.

We addressed the following questions. (1) Where is elastic energy stored in the merus? (2) How is energy storage affected when the saddle is severed? (3) Which mathematical model best characterizes the spring behavior? (4) How does elastic energy storage scale with body size and is there sexual dimorphism in elastic energy storage?

MATERIALS AND METHODS

Animal acquisition and maintenance

Gonodactylaceus falcatus (Forskål 1775) (Crustacea: Stomatopoda: Gonodactyloidea: Gonodactylidae; Fig. 1) were collected on Oahu, Hawaii in June 2008, brought to UC Berkeley, and kept for no longer than 4 months before the tests were performed. Eighteen *G. falcatus* were used for material tests and one female *G. falcatus* (26 mm total body length) was used for a computed tomography (CT) scan of one appendage. The animals were maintained in individual 2 l plastic cups with artificial sea water (salinity: 32–36 p.p.t.; 22°C) and were fed fresh grass shrimp twice per week. Three *Odontodactylus scyllarus* (Linnaeus 1758) (Crustacea: Stomatopoda: Gonodactyloidea: Odontodactylidae) were obtained from commercial vendors and maintained in individual 20 liter tanks (salinity: 32–36 p.p.t.; 22°C). *O. scyllarus* specimens were used for high speed videography of the mechanical tests.

Mineralization patterns of raptorial appendage

The mineralization of the merus was examined using micro-CT scans (model HMXST225, X-Tek, Tyngsboro Business Park, Massachusetts, USA) and three-dimensional (3-D) reconstruction software (VGStudio Max v. 2, Volume Graphics GmbH, Heidelberg, Germany). A freshly frozen individual *G. falcatus* was scanned at 6.50 µm slice thickness, 767×1238×867 Voxel size, 16 bit depth, 4.99 mm×8.05 mm×5.64 mm field of view, and 0.01 mm pixel^{-1} resolution. A maximum projection algorithm was used to visualize the mineralization patterns such that brighter coloration indicated greater material density. Isosurface rendering was used to show the 3-D surface conformation.

Preparation of specimens

The body size (length and mass) of each animal was measured and the lateral surface of the merus of both raptorial appendages was photographed (Nikon D300 SLR camera, AF micro Nikkor 60 mm lens; Nikon, Inc., Melville, NY, USA) to determine appendage dimensions (Fig. 3). The maximum span of the connective tissue between the meral-V and the main body of the merus, as well as the merus length from the most proximal edge to the most distal edge, were measured from each photograph (Sigmascan Pro 5.00, SPSS, Inc, Chicago, IL, USA). The maximum span of the connective tissue measured (Fig. 3) corresponded to the maximum natural contraction distance of the meral-V (Patek et al., 2007). Once removed from the animal, the appendages were kept wet with artificial salt water throughout the process to prevent dehydration.

A single appendage was randomly selected from each animal and mounted for use in a materials testing machine (Fig. 3). We mounted the merus with the proximal edge embedded in a mold of marine epoxy paste (PC.11 White epoxy paste; Protective Coating Co., PA, USA). The muscle tissue in the merus was physically removed using forceps just prior to mounting. After the epoxy was cured (10–18 h while submerged in artificial saltwater), we inserted a wire (304 stainless steel, 0.027 gauge; Malin Co., Cleveland, Ohio, USA) through a hole in the epoxy mold and attached it at the connection between the lateral extensor muscle apodeme and carpus. The wire hooked around and through the carpus and was glued along the dorsal side of the carpus, thereby providing a strong mechanical connection during spring compression. In addition, we glued (5-star Super Glue, Surehold, Chicago, IL, USA) the ventral sides of the carpus and merus together to prevent carpus rotation and simulate the latch system in intact appendages. This preparation was then mounted in a custom-built stainless steel cage that coupled the appendage preparation to the materials testing machine. The wire was clamped to the base of the materials testing machine and the steel cage was attached to the load cell (Fig. 3) (Blue Hill Instron model 5544; load cell model 2530-416, 0.5 kN maximum, 0.125 N resolution or 0.25% of load, Instron Corp., Canton, MA, USA).

Mechanical testing protocol for *G. falcatus*

Force–displacement curves were obtained as the materials testing machine moved the steel cage up at a set distance and speed; the upward movement of the materials testing machine and steel cage placed the load cell in tension and caused the wire to pull against the carpus to compress the merus (Fig. 3). The connection of the wire at the insertion point of the lateral extensor muscle allowed the wire to realistically actuate the proximal rotation of the meral-V around the pivot point along the lateral edge of the merus (Fig. 3). Velocity was held constant such that the total time of contraction was 700 ms, the approximate time of extensor muscle contraction prior to a strike *in vivo* (Burrows and Hoyle, 1972). Following a rapid and negligible deceleration of the materials testing machine, the appendage was brought back to a resting position with an equivalent speed. During these cycles, force–displacement pairs were digitally sampled at 500 samples s^{-1}. Each cycle was repeated 10 times with a minimum of 60 s between cycles to ensure adequate recovery time.

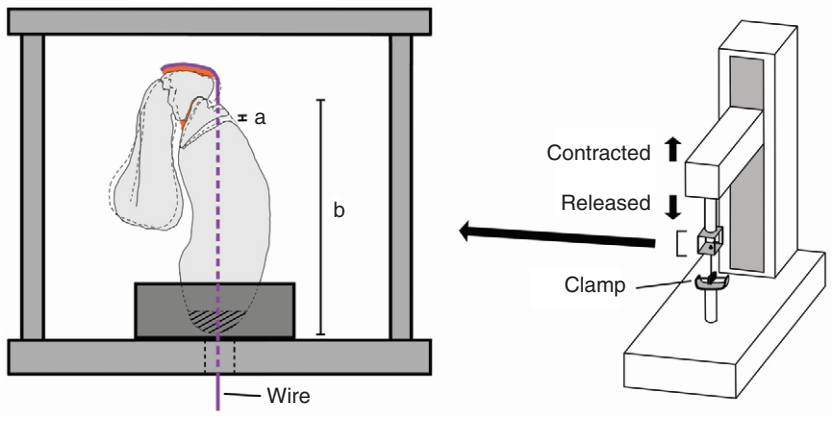

Fig. 3. Mechanical tests conducted using the second thoracopod of *G. falcatus*. The proximal edge of the exoskeleton (hatching) was cut to allow access to muscular tissue and run a wire (purple dashed line) through the merus. The wire was wrapped around and through the carpus (wire solid purple; glue orange) and emulated the connection point and orientation of the lateral extensor muscle, which typically compresses the merus. The load cell then measured the force required to compress the merus. The measurements used for calculating maximum contraction distance of the meral-V (a) and total merus length (b) are indicated.

We calculated system fatigue rate as the percent loss in maximum force over the course of 10 consecutive trials. We performed two additional tests on two appendages in order to assess fatigue and effects of contraction distance. For the first test, we contracted one appendage 60 times to calculate long-term experimental fatigue. Given that only minimal fatigue was observed (see Results), we then used the second appendage to assess the effect of total contraction distance on the slope or curvature of the force–displacement curve. In this test, we contracted the appendage to 100% of the calculated contraction distance for 10 cycles and then reduced the contraction to 50% for 10 cycles, then increased the contraction distance by 10%, 10 cycles each, until again reaching 100% contraction distance.

To determine if the saddle contributes to elastic energy storage in the merus, we measured the effect of severing the saddle in 10 appendages from 10 different individuals. For these tests, force was measured while the appendage was contracted 20 times in total, 10 times with an intact saddle, and then 10 times after a full incision was made across the saddle along the medial-lateral axis. To control for the effect of trial number on our results, seven appendages (from seven individuals) were cycled 20 times without cutting the saddle.

Data analysis and model fitting

We measured maximum force during compression, and calculated the slope of the force–displacement curve, area under the force–displacement curve, fatigue rate (as described above), and the effect of saddle incision on these parameters. The maximum force value for each test was recorded and then average maximum force across all test cycles performed on each individual was calculated.

Calculations were performed on a slightly truncated dataset. Owing to slack in the wire connecting the carpus to the materials testing machine, minimal force change occurred as the wire was pulled taut over the first 0–50 μm of the contraction (Fig. 4). Thus, we removed the initial 0–50 μm of each force–displacement curve before performing curve fitting calculations. In addition, occasional instability of the preparation was observed during the first one to three compression cycles of each test. We therefore conducted statistical analyses on both the complete datasets and the datasets with the first three compression cycles removed. The results were statistically nearly identical; thus, for the sake of brevity, we report here only the results of tests without the first three compression cycles.

We evaluated three models of the force–displacement curves,

linear: $$f(x) = Ax + B \quad (1)$$

exponential: $$f(x) = Ae^{Bx} + C \quad (2)$$

logistic: $$f(x) = \frac{A}{B + Ce^{Dx}} + E \quad (3)$$

with coefficients A, B, C, D as appropriate to each model and where x is the displacement of the meral-V during compression. For each individual, the force–displacement curve, least-squares residuals, coefficient of determination and the statistical deviance of the experimental data were calculated relative to the model fit for each of the three models (Curve fitting toolbox, Matlab v. 6, The Mathworks, Natick, MA, USA).

We then compared these three models using Akaike information criterion (AIC) (Akaike, 1981) which balances goodness of fit with parsimony. AIC was defined as the statistical deviance (log-likelihood ratio) plus two times the number of model parameters (implemented in Matlab v. 7). The model yielding the smallest AIC value indicates the most parsimonious and best-fit model among the three proposed models for each individual. To determine the best-supported model across all individuals, we calculated the proportion of tests across 18 intact appendages (before any saddle manipulations) for which each model was ranked as most parsimonious.

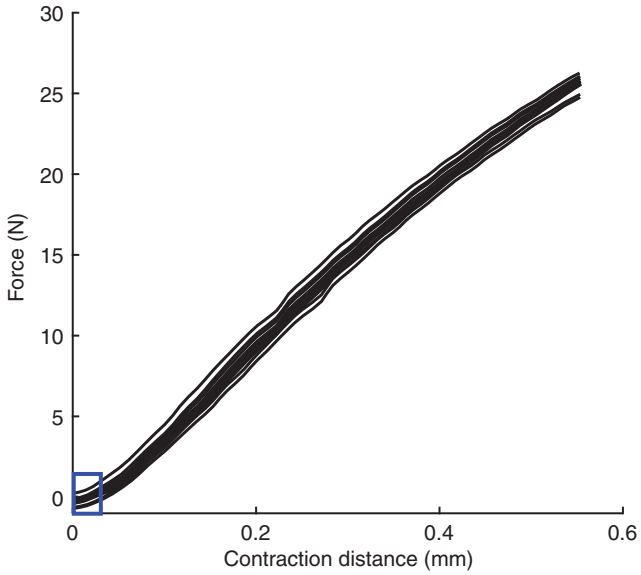

Fig. 4. The force–displacement curves from 10 consecutive compression cycles. At the start of the contraction, slack in the wire was taken up thereby resulting in a slightly lower slope (region in blue square). This region ranged from 0 to 50 μm and was removed for calculations of slope. The first cycle typically yielded the highest net force and subsequent cycles varied around a mean value such that fatigue rates typically averaged close to zero.

Given that the linear model was supported (see Results), we examined the scaling of maximum force and slope of the linear model with body size (body mass and merus length) using a least-squares linear curve fit (JMP, v. 7.0, SAS Institute, Cary, NC, USA). A t-test was used to test for the presence of sexual dimorphism in maximum contraction force and slope. The effect of saddle incision on maximum force, slope and fatigue rate was compared with preparations that had intact saddles, also using a t-test. We compared the area (work) under each force–displacement curve using spline interpolation (to facilitate numerical integration), to the area under the linear model of each force–displacement curve (Matlab v. 7.0).

We calculated resilience as the percent work during merus relaxation relative to the work required to contract the meral-V. Given that it was not possible to operate the materials testing machine at a speed that matches the extremely rapid release of the meral-V during an actual strike (Patek et al., 2004; Patek et al., 2007), we released the meral-V at the same rate with which it was compressed. Using data from the fifth contraction–release cycle of each appendage, we set the starting force to zero and calculated the area under the contraction and release curves between the location of zero-force during minimal displacement and the point at which the two curves crossed during maximal displacement (spline-interpolation; Matlab 7.0). We also calculated resilience during the fifteenth contraction–release cycle to compare individuals with severed and intact saddles.

Results are presented as mean ± 1 standard deviation.

High speed imaging of materials tests in *O. scyllarus*

In order to verify that the appendages were contracting in a biologically relevant manner, we collected high speed digital images (250–500 frames per second, 2–4 ms shutter duration, 1024×1024 pixel resolution; APX-RS high speed video camera, Photron Inc., San Diego, CA, USA) of compression tests performed on six appendages from three individuals under the same materials testing machine settings as used for *G. falcatus*. *O. scyllarus* were used instead of *G. falcatus*, because *O. scyllarus* have similar appendage morphology, but are about twice as large. Their greater size allowed us to more fully visualize the contraction dynamics. In addition, *O. scyllarus* strikes have been recorded in previous studies using high speed video (Patek et al., 2004; Patek and Caldwell, 2005; Patek et al., 2007) and thus could be compared to the movements observed in the compression tests. We filmed contractions from the medial, lateral and dorsal side of the appendage before and after the saddle was cut.

RESULTS

Mineralization patterns of raptorial appendage

Mineralization of the merus is confined to three primary regions (Figs 1 and 2). First, the ventral bar extends from a distal connection with the carpus, along the meral-V and proximally along the ventral surface of the merus. Second, medial bar runs ventrally to the saddle and connects to the carpus. Third, a ventral midline bar extends along the midline of the ventral surface of the merus. The saddle has small regions of mineralization at its distal and proximal edges.

Mechanical tests

With the saddle intact, the average maximum force required to compress the merus during the first 10 cycles ranged between 14.4 N and 40.1 N (mean 24.9±7.1 N; N=17). Maximum force was positively correlated with body size (Fig. 5; merus length: slope=2.1, d.f.=16, R^2=0.5610, F=19.17, P=0.0005; body mass: slope=0.66, d.f.=16, R^2=0.3913, F=9.64, P=0.0072) and meral-V displacement (slope=56.8, d.f.=16, R^2=0.6191, F=24.38, P=0.0002). Male appendages were significantly longer than those of females (N=17, d.f.=14.22, t=3.21, P=0.0062). Similarly, mean maximum force was greater in males than in females (N=17, d.f.=12.70, t=2.94, P=0.012).

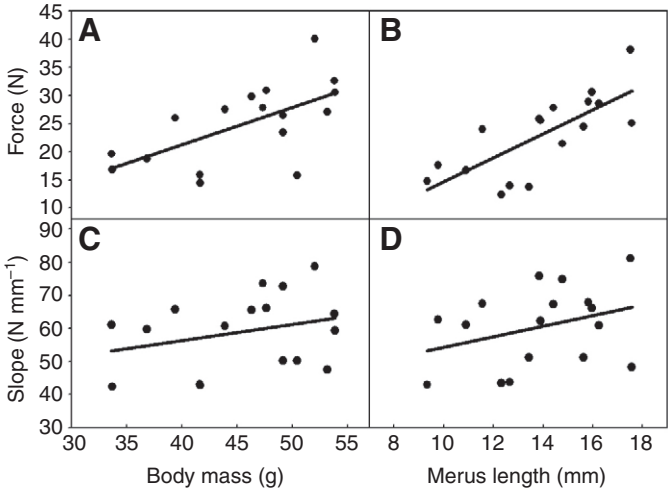

Fig. 5. Scaling of average maximum force (F) and slope (spring constant k) relative to body size. Average maximum force was positively correlated with both body mass (A) and merus length (B). Slope was not correlated with either body mass (C) or merus length (D).

The average fatigue rate of intact appendages was small (N=17, –0.2±0.4% cycle^{-1}) and the 60-cycle endurance test (N=1, 0.0±0.0% cycle^{-1}). Fatigue rate was similar after saddle incision (N=9, –0.3±0.8%).

We compared mean maximum force for individual appendages with intact saddles (cycles 4–10; the first three force–displacement cycles were removed – see Materials and methods) and after severing the saddle of the same appendages (cycles 14–20). In the control experiments, individuals with intact saddles throughout all cycles showed no significant changes in mean maximum force between cycles 4–10 and 14–20 (Fig. 6; mean cycles 4–10: 24.20 N, mean cycles 14–20: 24.20 N; paired t-test: d.f.=6, t=–0.055, P=0.96). Mean maximum force decreased significantly in individuals with a severed saddle in cycles 14–20 (Fig. 6; mean before saddle severed: 25.38 N, mean after saddle severed: 22.60 N; paired t-test: d.f.=9, t=5.28, P=0.0005). The second set of cycles in individuals with a severed saddle yielded 10.8±3.9% lower mean maximum force than when the saddle was intact.

Model fitting

There was no single favorable model; linear was ranked first in seven trials, exponential was ranked first in five trials and logistic was ranked first in six trials. In addition to being an acceptable choice from our AIC data, the linear model was a good fit as defined by R^2 values (except for one test, all R^2>0.95, 14 out of 18 R^2>0.99). We therefore used a linear spring model, following Hooke's law:

$$F = kx, \quad (4)$$

where F is the restoring force of the spring (equivalent to the force measured during our mechanical tests), the slope of the best fit line represents the spring constant k (a constant representing the stiffness of a particular spring where a higher value indicates a greater stiffness), and x is the distance over which the spring has been

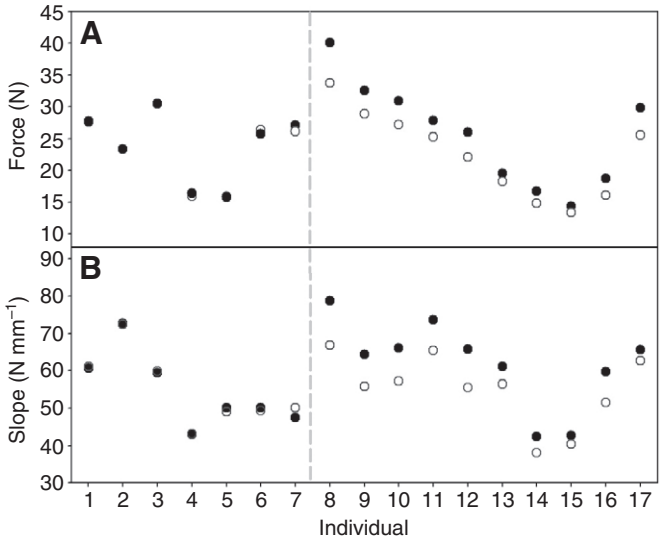

Fig. 6. The effect of saddle incision on force (F) and slope (spring constant k). One set of individuals (1–7) was tested for 10 cycles (filled circles) and then a second 10 cycles (outlined circles) without saddle incision. A second set of individuals (8–17) was tested for an initial ten cycles (filled circles), then the saddles were cut and the tests were run for a second set of ten cycles (outlined circles). Measurements of mean force (A) and slope (B) yielded significantly lower values after saddle incision. Untreated individuals showed no significant change in either parameter.

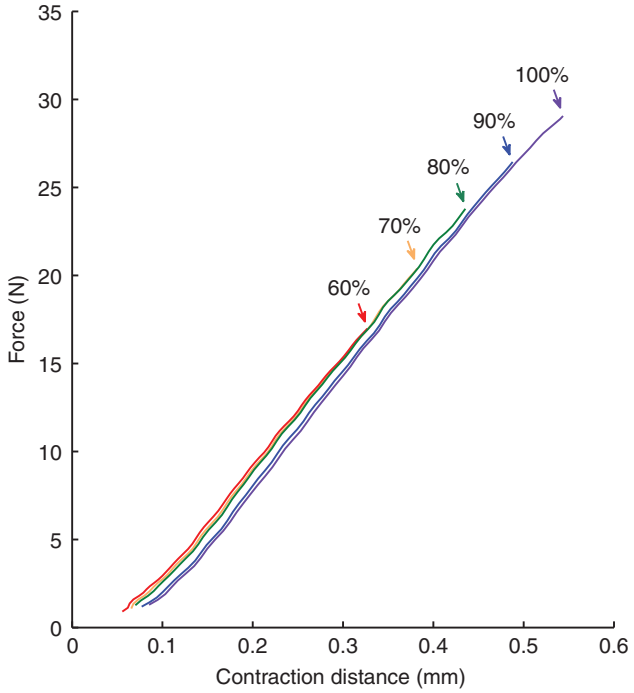

Fig. 7. Increasing contraction distance increased the maximum force, but did not change the slope of the force–displacement curve. Starting with red (60% of the full contraction distance), the contraction distance was incrementally increased [70% (orange), 80% (green), 90% (blue)] over ten-cycle increments until it reached the full contraction which was 100% of the meral-V span distance (purple).

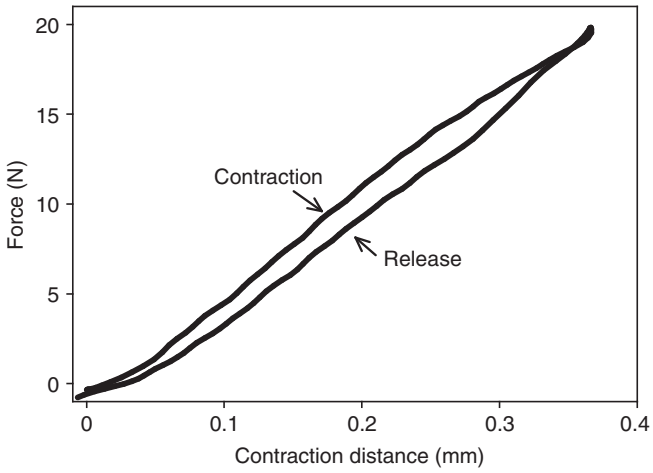

Fig. 8. A typical hysteresis curve during the fifth contraction–release cycle shows an average 81% resilience as calculated between the zero-crossing point at minimal contraction distance and the location at which the two curves cross at maximal contraction distance.

compressed or stretched (equal to the meral-V displacement; Fig. 3) (Ohanian, 1989).

The average spring constant with the saddle intact was 59.0±11.3 N mm^{-1} (N=17, range: 42.4–78.7). The spring constant k was not correlated with either body size (Fig. 5; least-squares linear regression: merus length: d.f.=16, R^2=0.1137, F=1.92, P=0.19; body mass: d.f.=16, R^2=0.0847, F=1.39, P=0.25) or sex (t-test: N=17, d.f.=10.44, t=0.63, P=0.54). Furthermore, the average spring constant was not dependent on the magnitude of the meral-V displacement, x, such that a cycle with a larger maximum contraction simply retraced and extended the previous cycle along an extension of the same line with the same slope (Fig. 7). Some possible creep was in evidence across these ten-cycle intervals (Fig. 7); however, creep was not observed in other repeated cycle tests. Finally, in the control experiments, k did not change across cycles in which the saddle was maintained intact (cycles 4–10: 57.38, cycles 14–20: 57.22, paired t-test: d.f.=6, t=0.61, P=0.56); however, it decreased significantly when the saddle was severed (cycles 4–10: 60.18, cycles 14–20: 53.76; paired t-test: d.f.=9, t=4.72, P=0.0011).

Calculations of work yielded a range of 1.6–10.3 mJ (mean 4.7±2.5 mJ, N=18) using the raw data and 1.1–10.3 mJ (mean 4.6±2.6 mJ, N=18) when calculated from the linear model fit. The linear model fit differed from the raw data calculation by an average 4.7±8.6%. Work decreased significantly after the saddle was cut (raw data: 4.3±2.7 mJ, paired t-test: d.f.=9, t=–3.72, P=0.005; model data: 4.1±2.7, paired t-test: d.f.=9, t=–2.61, P=0.028). The average decrease in work after the saddle cut was 11.0±4.9% when calculated from the raw data and 6.4±15.2% when calculated from the model. Work was positively correlated with body size (all tests including merus length, body mass, model and raw data yielded P<0.003).

Resilience averaged 81±7% (N=18; Fig. 8) during the fifth cycle and 84±7% during the fifteenth cycle (N=8) in appendages with intact saddles (no significant effect of cycle number: paired t-test, d.f.=7, t=0.11, P=0.915). Resilience decreased in severed saddles (77±11%), but not significantly (paired t-test, d.f.=9, t=–0.41, P=0.690). Neither body mass nor merus length were correlated with resilience (least-squares linear regression; P>0.1 in all tests).

High speed imaging of materials tests in *O. scyllarus*

High speed images of *O. scyllarus* revealed that both medial and lateral sides of the merus contract towards the proximal end of the appendage by a similar amount. On the lateral side, this contraction took place exclusively in the non-calcified space between the meral-V and the rest of the merus. On the medial side, the saddle contracted and the distal half of the merus bowed out medially, preventing the carpal–meral joint from rotating laterally. Once the saddle was severed, the dynamics of contraction changed. The carpal–meral joint initially started to rotate medially, as the destroyed saddle offered no resistance. Only after this short rotation did the merus begin to compress.

DISCUSSION

Elastic energy storage dynamics of mantis shrimp raptorial appendages can be effectively modeled as a Hookean spring. The spring constant (k) remained consistent across a range of body sizes while maximum force was positively correlated with body size. These results suggest that this system has a characteristic spring stiffness regardless of body size and that increases in force are generated by increasing the displacement distance (x) of the meral-V. The saddle only contributed a small proportion of the stored elastic energy, thus the ventral bars are most probably the primary location of elastic energy storage in this system.

Location of elastic energy storage

The merus segment is composed of paper-thin, poorly mineralized exoskeleton, several regions of arthrodial membrane, and the saddle. The primary mineralized regions are two ventral bars and a medial bar adjacent to the saddle, with a small region of mineralization at the distal and proximal limits of the saddle (Figs 1 and 2). Given

that cutting the saddle only reduced energy storage by 10%, the remaining mineralized bars appear to be the sites of elastic energy storage. As a preliminary experiment, we made an incision through the ventral bars while leaving the saddle intact, and then proceeded using the same settings as the tests in this study. The result was complete failure of the system and there was no observable resistance during compression of the merus, further supporting the role of these bars in elastic energy storage. Interestingly, these mineralization patterns are different from those previously observed in *O. scyllarus* (Patek et al., 2007). The ventral bars are similar; however, the medial bar is more discretely formed with a full extension to the carpus, unlike *O. scyllarus*, in which the bar is limited to the ventral edge of the saddle. Also, the ventral bar that extends along the meral-V appears to be more elaborate and extends to a connection point with the carpus, unlike in *O. scyllarus* where the mineralization ends before reaching the lateral carpus–meral joint. It must be noted that in both of these examples, only one specimen was subjected to a micro-CT scan. Therefore, these differences may be due to scaling or individual differences and may not be representative of each species.

The saddle is conserved across the order Stomatopoda (Ahyong, 1997; Ahyong and Harling, 2000) and may be integral to other aspects of this mechanism's function. The high speed imaging revealed that without an intact saddle, the carpus joint rotated medially and the medial side of the merus did not bow out as much as it did in intact specimens. Thus, the saddle may be necessary for inducing conformational changes during the strike that relieve mechanical stress. These conformational changes may be important for long-term durability and stability during the rapid acceleration and deceleration that the appendage experiences, both before and after contact with its prey.

Model of spring mechanics

Although the AIC did not yield consistent support for a single model, the linear Hookean model remained well-supported through regression analyses and also offered the simplest representation of the force–displacement curve. The correspondence between the work calculations made from the raw force–displacement curves as compared with the modeled relationships was close – an average of 4.7% difference between the two calculations.

Given that few studies have examined the mechanical dynamics of exoskeletal springs, we have little basis for comparison of the linear model to other possible models. Indeed, one key issue in the mantis shrimp is whether the spring behaves isotropically and returns the stored elastic energy in a similar linear behavior as we observed during loading. Certainly the loading and unloading regimes are distinct; loading occurs through the slow extensor muscle contraction (~700 ms) (Burrows, 1969) whereas unloading occurs in less than 2 ms when the latches are released prior to a strike (Patek et al., 2007). We measured 81% resilience when the merus was released at the same rate that it was contracted; until we develop a system to release the stored energy over 300 times more quickly, we remain uncertain whether this value accurately represents the energy storage in the system. Furthermore, as in cockroach legs (Dudek and Full, 2006), springs may play equally important roles in energy storage, release and stabilization and can work in concert with a dashpot to yield a spring-damper system.

There is little doubt, however, that the spring acts as a power amplifier. As work (and hence energy available) is given by the amount of force exerted times the distance over which this force acts, our work calculations lead us to a theoretical maximal strike energy for *G. falcatus*. Given the conservative estimate that the meral-V extends in less than 1.8 ms during a strike [based on high speed imaging of the much larger *O. scyllarus* (Patek et al., 2004; Patek et al., 2007)], the power output of this system would range from 0.9 to 5.7 W, with an average 2.6 W. Thus, with an average *G. falcatus* lateral extensor muscle weighing 97 mg, one can estimate the power output of the spring to be 27 kW kg^{-1} muscle. These values far exceed the highest known power outputs from muscles (around 1000 W kg^{-1} muscle) (Askew and Marsh, 2001; Alexander, 2002; Askew and Marsh, 2002) and indicate an efficacious power amplification mechanism in mantis shrimp.

Scaling of spring mechanics and the role of muscle constraints

An intriguing aspect of this system is found in the scaling of maximum force (F) and the spring constant (k). F was positively correlated with size and males had both larger appendages and greater maximum force than females. In contrast, k was statistically independent of measurements of body size and sex. Thus, returning to Hooke's Law (Eqn 4), as a mantis shrimp grows, the intrinsic stiffness of the spring, k, appears to stay relatively constant and larger individuals simply compress a similarly stiff spring further from its resting position to yield a greater force, F, that scales with body size.

The fact that k does not change across body size may point to the role of muscle constraints in this system and, by association, morphological changes in the spring across body size to accommodate a constant k. Previous studies of crustacean force generation and muscle output have noted a curious phenomenon: force is positively correlated with size, but muscle stress (force per unit area) is not (Taylor, 2000). Other studies have shown that in early development, crustaceans increase the length of their sarcomeres, but as adults they add more sarcomeres to lengthen muscle fibers and the sarcomeres do not increase in size (Govind et al., 1977; Haj et al., 1984). If we use the mantis shrimp's spring mechanics as a proxy for muscle mechanics, muscle work must increase across body size, but the force may not. This suggests that larger individuals may contract their extensor muscle over a greater distance (x), but maintain a constant force – possibly through increases in muscle fiber length (through addition of sarcomeres). If this is indeed the case, then the mantis shrimp's spring must increase in size concordantly with the body size-associated change in merus length while maintaining a constant k. Thus, to maintain a constant stiffness, the spring morphology must change in mineralization or shape over the size range of the mantis shrimp.

Another possibility is that exoskeletal elastic energy storage mechanics follow unexpected scaling relationships owing to the intrinsic properties of cylindrical systems with varying mineralization. Such intriguing scaling relationships were identified in the elastic energy storage mechanics of locust legs (Katz and Gosline, 1992; Katz and Gosline, 1994); the broader principles of arthropod elastic energy scaling mechanics have yet to be explored.

The interplay between material properties and shape determine elastic energy storage performance in biological systems (Wainwright et al., 1976; Vincent and Wegst, 2004). Although we have assessed the behavior of this system, the essential issues of underlying material composition and the shape of the ventral bars and saddle remain unexplored. One remarkably similar system is found in froghoppers, which flex 'pleural arches' to store energy prior to their high-powered jumps (Burrows et al., 2008). Parts of the arches are impregnated with resilin, which gives them flexibility, while the arches themselves provide the necessary stiffness to store

up sufficient elastic energy. Burrows et al. (Burrows et al., 2008) make the compelling argument that, not only does resilin contribute to the elasticity of the structure, it also decreases creep, reduces vibration and maintains mechanical properties. Resilin has not yet been identified in stomatopods, but the similarities between the ventral bars in mantis shrimp and pleural arches in insects suggest possible unexplored roles of other materials in this system.

To conclude, the mantis shrimp's raptorial spring is a potent power amplifier and highly integrated exoskeletal structure. The scaling relationships of maximum force and spring constant suggest a possible role of muscle constraints in spring design; further studies of the scaling of spring mechanics may yield key insights into the selective and scaling processes involved in the evolution of this system. Exoskeletal spring mechanics are critical to fast movements throughout the arthropods, yet few studies have tackled the mechanical and dynamic behavior of these structures. The compelling combinations of materials and shape found in previous studies and the intriguing mechanical dynamics found in the mantis shrimp's elastic system, suggest a rich and relatively untapped biomechanical history of fast animal movements.

CT scans were performed at the Center for Nanoscale Systems at Harvard University, a member of the National Nanotechnology Infrastructure Network (National Science Foundation award # ECS-0335765). Materials tests were performed at the Center for Integrative Biomechanics in Education and Research at the University of California, Berkeley. We thank T. F. Kosar, T. Libby and S. Sponberg for technical assistance, E. Staaterman and R. Caldwell for animal collection, M. Mendoza for muscle measurements, J. R. A. Taylor for comments on the manuscript, and Patek Laboratory members for feedback and assistance with animal care. This research was supported by the UC Berkeley Undergraduate Research Apprenticeship Program (to T.I.Z.), the National Science Foundation (award # 0641716 to S.N.P.) and the Radcliffe Institute for Advanced Study (to S.N.P.).

REFERENCES

Ahyong, S. T. (1997). Phylogenetic analysis of the Stomatopoda (Malacostraca). *J. Crust. Biol.* **17**, 695-715.
Ahyong, S. T. and Harling, C. (2000). The phylogeny of the stomatopod Crustacea. *Aust. J. Zool.* **48**, 607-642.
Akaike, H. (1981). Likelihood of a model and information criteria. *J. Econom.* **16**, 3-14.
Alexander, R. M. (1983). *Animal mechanics.* Boston: Blackwell Scientific Publications.
Alexander, R. M. (1984). Elastic energy stores in running vertebrates. *Am. Zool.* **24**, 85-94.
Alexander, R. M. (1990). Elastic mechanisms in the locomotion of vertebrates. *Neth J. Zool.* **40**, 93-105.
Alexander, R. M. (2002). Tendon elasticity and muscle function. *Comp. Biochem. Physiol.* **133A**, 1001-1011.
Alexander, R. M. and Bennet-Clark, H. C. (1977). Storage of elastic strain energy in muscle and other tissues. *Nature* **265**, 114-117.
Askew, G. N. and Marsh, R. L. (2001). The mechanical power output of the pectoralis muscle of blue-breasted quail (*Coturnix chinensis*): the *in vivo* length cycle and its implications for muscle performance. *J. Exp. Biol.* **204**, 3587-3600.
Askew, G. N. and Marsh, R. L. (2002). Muscle designed for maximum short-term power output: quail flight muscle. *J. Exp. Biol.* **205**, 2153-2160.
Asmussen, G. and Marechal, G. (1989). Maximal shortening velocities, isomyosins and fiber types in soleus muscle of mice, rats and guinea-pigs. *J. Physiol.* **416**, 245-254.
Bennet-Clark, H. C. (1975). The energetics of the jump of the locust *Schistocerca gregaria*. *J. Exp. Biol.* **63**, 53-83.
Bennet-Clark, H. C. (1976a). *Energy Storage in Jumping Animals.* Oxford, New York, Toronto, Sydney, Paris, Braunschweig: Pergamon Press.
Bennet-Clark, H. C. (1976b). Energy storage in jumping insects. In *The Insect Integument* (ed. H. R. Hepburn), pp. 421-443. Amsterdam: Elsevier Scientific Publishing Company.
Bennet-Clark, H. C. and Lucey, E. C. A. (1967). The jump of the flea: a study of the energetics and a model of the mechanism. *J. Exp. Biol.* **47**, 59-76.
Blickhan, R. (1989). The spring mass model for running and hopping. *J. Biomech.* **22**, 1217-1227.
Blickhan, R. and Full, R. J. (1993). Similarity in multilegged locomotion – bouncing like a monopode. *J. Comp. Physiol. A* **173**, 509-517.
Brackenbury, J. and Hunt, H. (1993). Jumping in springtails: mechanism and dynamics. *J. Zool.* **229**, 217-236.
Burrows, M. (1969). The mechanics and neural control of the prey capture strike in the mantid shrimps *Squilla* and *Hemisquilla*. *Z. vergleichende Physiol.* **62**, 361-381.
Burrows, M. (2007). Kinematics of jumping in leafhopper insects (Hemiptera, Auchenorrhyncha, Cicadellidae). *J. Exp. Biol.* **210**, 3579-3589.
Burrows, M. and Hoyle, G. (1972). Neuromuscular physiology of the strike mechanism of the mantis shrimp, *Hemisquilla*. *J. Exp. Zool.* **179**, 379-394.
Burrows, M. and Sutton, G. P. (2008). The effect of leg length on jumping performance of short- and long-legged leafhopper insects. *J. Exp. Biol.* **211**, 1317-1325.
Burrows, M., Shaw, S. and Sutton, G. (2008). Resilin and chitinous cuticle form a composite structure for energy storage in jumping by froghopper insects. *BMC Biology* **6**, 41.
Currey, J. D., Nash, A. and Bonfield, W. (1982). Calcified cuticle in the stomatopod smashing limb. *J. Mat. Sci.* **17**, 1939-1944.
Dudek, D. M. and Full, R. J. (2006). Passive mechanical properties of legs from running insects. *J. Exp. Biol.* **209**, 1502-1515.
Govind, C. K., She, J. and Lang, F. (1977). Lengthening of lobster muscle fibres by two age-dependent mechanisms. *Experientia* **33**, 35-36.
Gravish, N., Wilkinson, M. and Autumn, K. (2008). Frictional and elastic energy in gecko adhesive detachment. *J. R. Soc. Interface* **5**, 339-348.
Gronenberg, W. (1996). Fast actions in small animals: springs and click mechanisms. *J. Comp. Physiol.* **178**, 727-734.
Haj, A. J. E., Govind, C. K. and Houlihan, D. F. (1984). Growth of lobster leg muscle fibers over intermolt and molt. *J. Crustacean Biol.* **4**, 536-545.
Heitler, W. J. (1974). The locust jump: specialisations of the metathoracic femoral-tibial joint. *J. Comp. Physiol.* **89**, 93-104.
James, R. S., Navas, C. A. and Herrel, A. (2007). How important are skeletal muscle mechanics in setting limits on jumping performance? *J. Exp. Biol.* **210**, 923-933.
Jensen, M. and Weis-Fogh, T. (1962). Biology and physics of locust flight. V. strength and elasticity of locust cuticle. *Philos. Trans. R. Soc. London* **245**, 137-169.
Josephson, R. K. (1993). Contraction dynamics and power output of skeletal muscle. *Ann. Rev. Physiol.* **55**, 527-546.
Josephson, R. K. and Stokes, D. R. (1994). Contractile properties of a high-frequency muscle from a crustacean III. Mechanical power output. *J. Exp. Biol.* **187**, 295-303.
Katz, S. L. and Gosline, J. M. (1992). Ontogenetic scaling and mechanical behaviour of the tibiae of the African desert locust (*Schistocerca gregaria*). *J. Exp. Biol.* **168**, 125-150.
Katz, S. and Gosline, J. (1994). Scaling modulus as a degree of freedom in the design of locust legs. *J. Exp. Biol.* **187**, 207-223.
McNeill, P., Burrows, M. and Hoyle, G. (1972). Fine structures of muscles controlling the strike of the mantis shrimp, *Hemisquilla*. *J. Exp. Zool.* **179**, 395-416.
Ohanian, H. C. (1989). *Physics.* New York: W. W. Norton and Company.
Patek, S. N. and Caldwell, R. L. (2005). Extreme impact and cavitation forces of a biological hammer: strike forces of the peacock mantis shrimp (*Odontodactylus scyllarus*). *J. Exp. Biol.* **208**, 3655-3664.
Patek, S. N., Korff, W. L. and Caldwell, R. L. (2004). Deadly strike mechanism of a mantis shrimp. *Nature* **428**, 819-820.
Patek, S. N., Nowroozi, B. N., Baio, J. E., Caldwell, R. L. and Summers, A. P. (2007). Linkage mechanics and power amplification of the mantis shrimp's strike. *J. Exp. Biol.* **210**, 3677-3688.
Pennycuick, C. J. (1968). Power requirements for the horizontal flight in pigeon *Columba livia*. *J. Exp. Biol.* **49**, 527-555.
Raabe, D., Sachs, C. and Romano, P. (2005). The crustacean exoskeleton as an example of a structurally and mechanically graded biological nanocomposite material. *Acta Mater.* **53**, 4281-4292.
Roberts, T. J. and Marsh, R. L. (2003). Probing the limits to muscle-powered accelerations: lessons from jumping bullfrogs. *J. Exp. Biol.* **206**, 2567-2580.
Rothschild, M., Schlein, Y., Parker, K. and Sternberg, S. (1972). Jump of the oriental rat flea *Xenopsylla cheopis* (Roths.). *Nature* **239**, 45-48.
Sachs, C., Fabritius, H. and Raabe, D. (2006). Experimental investigation of the elastic-plastic deformation of mineralized lobster cuticle by digital image correlation. *J. Struct. Biol.* **155**, 409-425.
Seffen, K. A. and Pellegrino, S. (1999). Deployment dynamics of tape springs. *Proc. R. Soc. London Ser. A* **455**, 1003-1048.
Taylor, G. M. (2000). Maximum force production: why are crabs so strong? *Proc. R. Soc. London B* **267**, 1475-1480.
Vincent, J. F. V. and Wegst, U. G. K. (2004). Design and mechanical properties of insect cuticle. *Arthropod Struct. Dev.* **33**, 187-199.
Wainwright, S. A., Biggs, W. D., Currey, J. D. and Gosline, J. M. (1976). *Mechanical Design in Organisms.* Princeton: Princeton University Press.